

Stable dark and bright soliton Kerr combs can coexist in normal dispersion resonators

Pedro Parra-Rivas^{1,2}, Damià Gomila², and Lendert Gelens^{1,3,*}

¹*Applied Physics Research Group, Vrije Universiteit Brussel, 1050 Brussels, Belgium*

²*IFISC institute (CSIC-UIB), Campus Universitat de les Illes Balears, E-07122 Palma de Mallorca, Spain*

³*Laboratory of Dynamics in Biological Systems, KU Leuven, Department of Cellular and Molecular Medicine, University of Leuven, B-3000 Leuven, Belgium*

* *Corresponding author: lendert.gelens@kuleuven.be*

Compiled October 1, 2018

Using the Lugiato-Lefever model, we analyze the effects of third order chromatic dispersion on the existence and stability of dark and bright soliton Kerr frequency combs in the normal dispersion regime. While in the absence of third order dispersion only dark solitons exist over an extended parameter range, we find that third order dispersion allows for stable dark and bright solitons to coexist. Reversibility is broken and the shape of the switching waves connecting the top and bottom homogeneous solutions is modified. Bright solitons come into existence thanks to the generation of oscillations in the switching wave profiles. Finally, oscillatory instabilities of dark solitons are also suppressed in the presence of sufficiently strong third order dispersion.

© 2018 Optical Society of America

The Lugiato-Lefever [1] equation (LLE) has attracted a lot of interest in the last few years for describing the generation of Kerr frequency combs in high-Q microresonators driven by a continuous-wave (CW) laser [2, 4]. These frequency combs can be integrated on chip [3] and used to measure time intervals and light frequencies with an exquisite accuracy, leading to numerous key applications [5–9]. In this framework a Kerr frequency comb corresponds to the frequency spectrum of a temporal dissipative structure, such as patterns or solitons, circulating inside the cavity [10, 11]. While most theoretical studies have focused on the anomalous second-order group velocity dispersion (GVD) regime [12–14], where the typical dissipative states are bright solitons, the normal GVD regime has recently attracted interest due to the difficulty of obtaining anomalous GVD in some spectral ranges. In contrast to the anomalous regime, dark solitons are found in the normal GVD regime, i.e. low-intensity dips embedded in a high-intensity homogeneous background. The bifurcation structure and temporal dynamics of these dark solitons, also called “platicons”, have been recently studied [15–17], and their origin is intimately related with the locking of switching waves (SWs) connecting co-existing homogeneous state solutions of high and low intensity [16, 17]. The generation of such dark pulse Kerr frequency combs has been achieved experimentally by several groups [18–20].

In the anomalous GVD regime it was shown that high-order chromatic dispersion effects can modify the dynamics and bifurcation structure of solitons in the LLE [21]. In particular, third-order dispersion (TOD) generates the emission of dispersive waves that can lead to the suppression of dynamical regimes such as oscillations and chaos [22, 23]. As TOD also breaks reversibility, solitons move with a constant velocity [22–26]. While recent work has numerically shown that TOD induces similar dispersive waves in dark solitons [27], studies of the influence of TOD in the normal GVD regime remain scarce.

In this letter we present a detailed analysis of the bifurca-

tion structure of soliton Kerr combs in the normal dispersion regime in the presence of TOD. In particular we show that stable bright and dark solitons coexist over an increasingly wide parameter range for increasing values of TOD, and we explain such soliton stabilization by analyzing the shape of SWs of different polarities whose locking lies at the heart of this phenomenon. Using the normalization of [28], the LLE reads

$$\partial_t u = -(1 + i\theta)u + iu|u|^2 + u_0 - i\partial_\tau^2 u + d_3 \partial_\tau^3 \quad (1)$$

where t is the slow time describing the evolution of the intracavity field $u(t, \tau)$ on the time scale of the cavity photon lifetime and τ is the fast time that describes the temporal structure for the field on the time scale of the resonator round trip L . The first term on the right-hand side describes cavity losses (the system is dissipative by nature); u_0 is the amplitude of the homogeneous (CW) driving field or pump; θ measures the cavity frequency detuning between the frequency of the input pump and the nearest cavity resonance; ∂_τ^2 models the GVD (here assumed to be normal at the pump frequency); $d_3 \partial_\tau^3$ models the TOD and d_3 is its strength; and the sign of the cubic term is set so that it corresponds to the self-focusing Kerr nonlinearity.

For $\theta > \sqrt{3}$, three homogeneous steady state (HSS) solutions exist: u_t (a stable HSS of higher intensity), u_m (an unstable saddle HSS of intermediate intensity), and u_b (a stable HSS of lower intensity). Figure 1 illustrates how the system can relax into different stable structures depending on the initial condition. In the absence of TOD, Figure 1(a) shows that a dip in the high intensity HSS u_t (red) can evolve into a stable dark soliton (black), while a bump on the low intensity HSS u_b (red) relaxes back to u_b . This observation that dark solitons exist, but bright solitons do not, is general [15–17]. Ref. [16] discussed that dark solitons exist due to the locking of overlapping oscillatory tails in the profile of SWs connecting the upper state u_t to the bottom state u_b . As such oscillations are absent in SWs approaching the upper state u_t , bright solitons do not exist (apart from at one single value of the

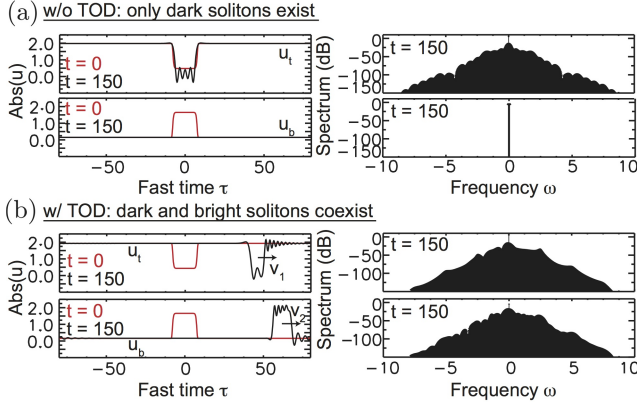


Fig. 1. Solution profile at $t = 150$ (black) after time evolution in the LLE (1) of an initial dip in the top HSS u_t or a bump on the bottom HSS u_b (red) in the absence (a) or presence of TOD (b). Left panels show the time profile, while the right panels show its associated comb spectrum. Parameter set: (a) $(\theta, u_0, d_3) = (4, 2.175, 0)$; (b) $(\theta, u_0, d_3) = (4, 2.3, 0.7)$.

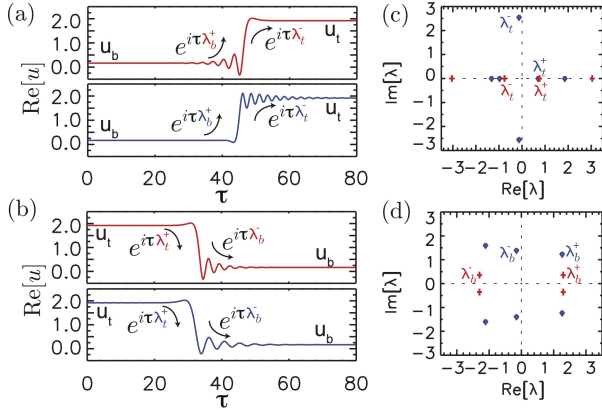


Fig. 2. Switching waves SW_u (a) and SW_d (b), in each case for $d_3 = 0$ (top panel, red) and $d_3 = 0.7$ (bottom panel, blue). The spatial eigenvalues corresponding to u_t and u_b are shown in (c) and (d), respectively, both for $d_3 = 0$ (red crosses) and $d_3 = 0.7$ (blue diamonds). $u_0 = 2.32529$.

pump, called the Maxwell point u_0^M [16]). Figure 1(b) shows a similar numerical simulation, but now in the presence of TOD ($d_3 = 0.7$). The initial condition corresponding to a dip still evolves to a dark soliton, which now has an asymmetric profile that moves at velocity v_1 while stably maintaining its temporal shape and corresponding frequency spectrum. However, in contrast to the case without TOD, an initial bump now no longer relaxes to the HSS u_b , but it forms a bright soliton corresponding to a fixed profile moving at velocity v_2).

As already suggested, analyzing the shape of the SWs connecting HSSs u_t and u_b is key to understanding why dark and bright solitons can stably coexist in the presence of TOD. Figure 2(a) shows the shape of an up-switching wave SW_u connecting the low intensity HSS u_b to the high intensity HSS u_t , both in the absence (red) and presence (blue) of TOD. Figure 2(b) similarly shows the profile of the opposite down-

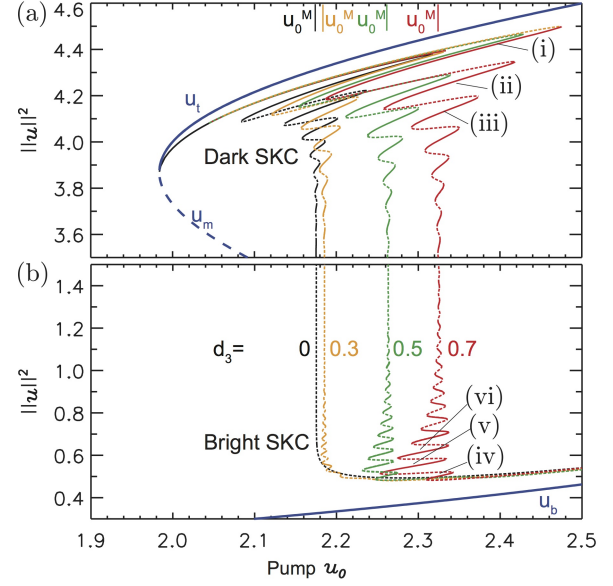


Fig. 3. Bifurcation diagrams of HSSs (blue) and dark and bright solitons for $\theta = 4$ and increasing values of $d_3 = 0$ (black), 0.3 (yellow), 0.5 (green), 0.7 (red). Solid (dashed) lines correspond to stable (unstable) states.

switching wave SW_d , connecting the high intensity HSS u_t to the low intensity HSS u_b . Figures 2(c)-(d) plot the corresponding "spatial eigenvalues λ " of the linearized stationary problem around each HSS, which can be determined analytically [29, 30]. The damping rate q and the frequency Ω of the oscillatory tails around u_t and u_b correspond to the real and imaginary part of certain spatial eigenvalues λ . The approach to the top HSS u_t by SW_u and the departure from u_t by SW_d can be approximated linearly in the form $SW_{u,d}(\tau) - u_t \propto e^{\lambda_t^{\pm} \tau}$, where the λ_t is each time the leading spatial eigenvalue. Similarly, the approach to and departure from the bottom HSS u_b is approximated by $SW_{u,d}(\tau) - u_b \propto e^{\lambda_b^{\pm} \tau}$.

Without TOD, the system is reversible under the transformation $\tau \rightarrow -\tau$. As a consequence spatial eigenvalues (red) come in pairs and are symmetric respect to both axes $\text{Re}[\lambda]=0$ and $\text{Im}[\lambda]=0$. This means that both SW_u (a) and SW_d (b) approach and leave u_t and u_b in the same way. The top HSS u_t is always approached/left in a monotonic way, explained by the corresponding purely real spatial eigenvalues. In contrast, the bottom HSS u_b is always approached/left in an oscillatory fashion, because its corresponding spatial eigenvalues are complex. Such oscillations can interlock around u_b to form stable dark solitons, but the absence of similar oscillations around u_t prevent stable bright solitons to form. When adding TOD, the dynamics around the HSSs are described by six eigenvalues instead of four, and they are no longer symmetric. The shape of the SW s changes in such a way that they now approach/leave the HSSs u_t in an oscillatory way. Therefore locking can occur not only in the bottom HSS u_b but also in the top one u_t , forming bright solitons.

In Fig. 3 we plot, using the mean energy $\|u\|^2 \equiv L^{-1} \int_0^L |u|^2 d\tau$, the bifurcation diagrams of HSSs and soli-

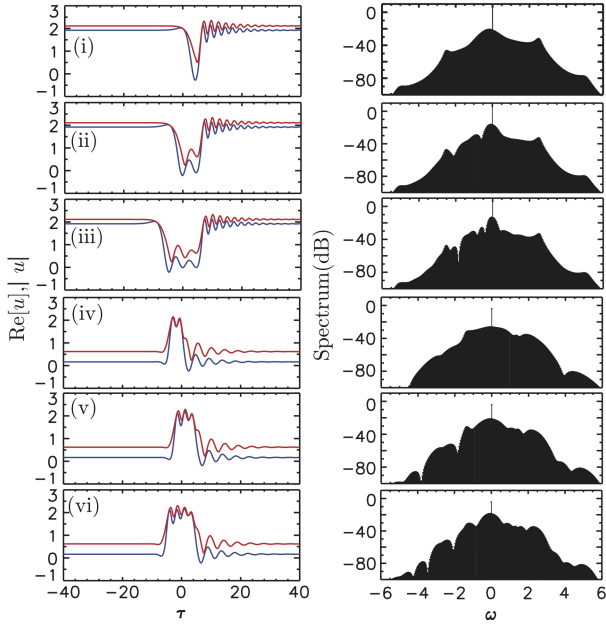


Fig. 4. Temporal profiles [left; $\text{Re}(u)$ in blue, $|u|$ in red] and spectral intensities (right, in dB) of asymmetric dark and bright solitons corresponding to the locations (i)-(iii) and (iv)-(vi) in Fig. 3. $(\theta, u_0, d_3) = (4, 2.232, 0.7)$.

tons in function of the pump amplitude u_0 for $d_3 = 0$ and increasing values of d_3 . In blue, the three HSS solutions are shown. In black, the bifurcation diagram of dark solitons is shown for $d_3 = 0$ and has been discussed in detail in [16,17]. Unstable (dashed line) dark solitons originate from the saddle-node point $\text{SN}_{\text{hom},2}$ and acquire stability (solid line) at the next turning point when increasing the pump amplitude. Dark solitons of increasing width, corresponding to branches with lower mean energy, exist over a parameter range (u_0) that becomes narrower and narrower, eventually collapsing to the Maxwell point of the system at u_0^M . These dark solitons are connected by unstable solution branches that serve to add additional spatial oscillations in their profiles, leading to the broadening of the dark states. This type of bifurcation structure is called a *collapsed snaking* structure. When TOD is taken into account, SW_u gradually develops oscillations, which allows bright solitons to come into existence. This can be seen in Fig. 3(b) in yellow ($d_3=0.3$) where bright solitons now exist over a narrow range of pump values u_0 . Increasing d_3 further, the spatial oscillations in SW_u become stronger, leading to the stabilization of bright solitons over a wider range of pump parameters ($d_3=0.5$ (green), 0.7 (red)). Fig. 3(a) shows that also the dark solitons exist over a wider range of parameters, and the Maxwell point u_0^M (around which the collapsed snaking structure is organized) shifts to higher values of the pump u_0 . Typical solution profiles of solitons corresponding to different branches are plotted in Figure 4 for $d_3=0.7$ (red). In the presence of TOD, both dark [Figure 4(i)-(iii)] and bright [Figure 4(iv)-(vi)] solitons exist over an increasingly narrow parameter range as they increase their width.

For $d_3 = 0$, at higher values of the detuning θ dark soli-

tons have been shown to undergo Hopf instabilities and period doubling bifurcations starting a route to temporal chaos [16, 17]. This scenario is similar to the one regarding bright solitons in the anomalous dispersion regime [12, 13]. In that regime, it was shown that TOD, which leads to drift instabilities, could suppress such oscillatory and chaotic temporal dynamics of bright solitons [23]. We found that this mechanism of stabilization is also present in the normal dispersion regime. To illustrate this we first show the bifurcation diagram for $\theta = 5$ and $d_3 = 0$ in Fig. 5(a). Dark solitons are unstable between H_1 and H_2 leading to temporal oscillations. When $d_3 \neq 0$, the Hopf bifurcations shift in such way that the oscillatory region shrinks for increasing values of TOD until it disappears (see Fig. 5(b)-(d) for $d_3 = 0.2, 0.3$ and 0.7 respectively). While for $d_3 = 0.2$, dark solitons between H_1 and H_2 oscillate and drift, for $d_3 = 0.3$ and 0.7 the oscillatory instabilities have been suppressed and only a drifting soliton remains. The direction in which the soliton drifts is not obvious by looking at its profile and changes with the pump u_0 . In Fig. 5, solid purple (green) lines correspond to dark solitons with positive (negative) velocity, while the solid red lines (for $d_3 = 0$) indicate zero velocity. By increasing the strength of TOD, the parameter range of solitons with negative velocity shrinks. Although in principle bright solitons could also undergo oscillatory instabilities and similar stabilization with increasing TOD, for the parameter range considered in this work, no such oscillations of bright solitons have been found.

The velocity of solitons is not solely determined by the system parameters, but also varies with the width and shape of the soliton. This is illustrated in Fig. 6(a)-(b), where two dark solitons of different width travel at different speeds and thus unavoidably interact upon collision. Two dark solitons are dissipative structures and do not come out of such a collision unchanged such as the classical solitons in conservative systems. Instead, a new wider soliton [Fig. 6(a)] or a bound state of both solitons [Fig. 6(b)] can be created. Fig. 6(c)-(d) shows the interaction of several bright and dark domains for two different values of the pump power. In Fig. 6(c) the pump is below the Maxwell point u_0^M , such that the bottom HSS is favored and a combination of bright solitons result, while in Fig. 6(d) the pump is above u_0^M , such that the top HSS is dominant and the formation of dark solitons is favored.

In summary, we have presented a bifurcation analysis of solitons and their corresponding Kerr combs in the normal GVD regime in the presence of TOD. Bright solitons have been shown to be stable over a wide parameter region due to locking of SWs. TOD can create such oscillatory tails in the SWs around the high intensity HSS u_r . Both dark and bright solitons are organized in a collapsed snaking bifurcation diagram, such that broader solitons always exist over a narrower parameter region. Furthermore, TOD can suppress oscillatory and chaotic instabilities of dark solitons in a similar fashion than for the anomalous case. Finally, we have shown that solitons of different widths propagate at different velocity, and multiple different solitons in a resonator thus eventually collide inelastically to form new solitons.

We acknowledge support from the Research Foundation—Flanders (FWO-Vlaanderen) (PPR), the Belgian Science

Policy Office (BelSPO) under Grant IAP 7-35, the Research Council of the Vrije Universiteit Brussel, the Spanish MINECO and FEDER under Grant ESOTECOS (FIS2015-63628-C2-1-R) (DG).

References

1. L. A. Lugiato and R. Lefever, *Phys. Rev. Lett.* **58**, 2209–2211 (1987).
2. P. Del’Haye, A. Schliesser, O. Arcizet, T. Wilken, R. Holzwarth, and T. J. Kippenberg, *Nature* **450**, 1214–1217 (2007).
3. V. Brasch, M. Geiselmann¹, T. Herr¹, G. Lihachev, M. H. P. Pfeiffer, M. L. Gorodetsky, and T. J. Kippenberg, *Science* **351**, 357 (2016).
4. T. J. Kippenberg, R. Holzwarth, and S. A. Diddams, *Science* **332**, 555–559 (2011).
5. Y. Okawachi, K. Saha, J. S. Levy, Y. H. Wen, M. Lipson, and A. L. Gaeta, *Opt. Lett.* **36**, 3398–3400 (2011).
6. S. B. Papp, K. Beha, P. Del’Haye, F. Quinlan, H. Lee, K. J. Vahala, and S. A. Diddams, *Optica* **1**, 10–14 (2014).
7. F. Ferdous, H. Miao, D. E. Leaird, K. Srinivasan, J. Wang, L. Chen, L. T. Varghese, and A. M. Weiner, *Nature Photon.* **5**, 770–776 (2011).
8. T. Herr, K. Hartinger, J. Riemensberger, C. Y. Wang, E. Gavartin, R. Holzwarth, M. L. Gorodetsky, and T. J. Kippenberg, *Nature Photon.* **6**, 480–487 (2012).
9. J. Pfeifle, V. Brasch, M. Laueremann, Y. Yu, D. Wegner, T. Herr, K. Hartinger, P. Schindler, J. Li, D. Hillerkuss, R. Schmogrow, C. Weimann, R. Holzwarth, W. Freude, J. Leuthold, T. J. Kippenberg, and C. Koos, *Nature Photon.* **8**, 375–380 (2014).
10. S. Coen, H. G. Randle, T. Sylvestre, and M. Erkintalo, *Opt. Lett.* **38**, 37–39 (2013).
11. Y. K. Chembo and C. R. Menyuk, *Phys. Rev. A* **87**, 053852 (2013).
12. F. Leo, L. Gelens, P. Emplit, M. Haelterman, and S. Coen, *Opt. Expr.* **21**, 9180 (2013).
13. P. Parra-Rivas, D. Gomila, M. A. Matías, S. Coen, and L. Gelens, *Phys. Rev. A* **89**, 043813 (2014).
14. C. Godey, I. V. Balakireva, A. Coillet, and Y. K. Chembo, *Phys. Rev. A* **89**, 063814 (2014).
15. V.E. Lobanov, G. Lihachev, T. J. Kippenberg, and M.L. Gorodetsky, *Opt. Expr.* **23**, 7713–7721 (2015).
16. P. Parra-Rivas, D. Gomila, E. Knobloch, S. Coen and L. Gelens, *Opt. Lett.* **41**, 2402–2405 (2016).
17. P. Parra-Rivas, E. Knobloch, D. Gomila, L. Gelens, *Phys. Rev. A* **93**, 063839 (2016).
18. W. Liang, A. A. Savchenkov, V. S. Ilchenko, D. Eliyahu, D. Seidel, A. B. Matsko, and L. Maleki, *Opt. Lett.* **39**, 2920–2923 (2014).
19. S.-W. Huang, H. Zhou, J. Yang, J. F. McMillan, A. Matsko, M. Yu, D.-L. Kwong, L. Maleki, and C. W. Wong, *Phys. Rev. Lett.* **114**, 053901 (2015).
20. X. Xue, Y. Xuan, Y. Liu, P.-H. Wang, S. Chen, J. Wang, D. E. Leaird, M. Qi, and A. M. Weiner, *Nature Photon.* **9**, 594–600 (2015).
21. M. Tlidi and L. Gelens, “High-order dispersion stabilizes dark dissipative solitons in all-fiber cavities,” *Opt. Lett.* **35**, 306 (2010).
22. C. Milián and D. Skryabin, “Soliton families and resonant radiation in a micro-ring resonator near zero group-velocity dispersion,” *Opt. Expr.* **22**, 3732–3739 (2014).

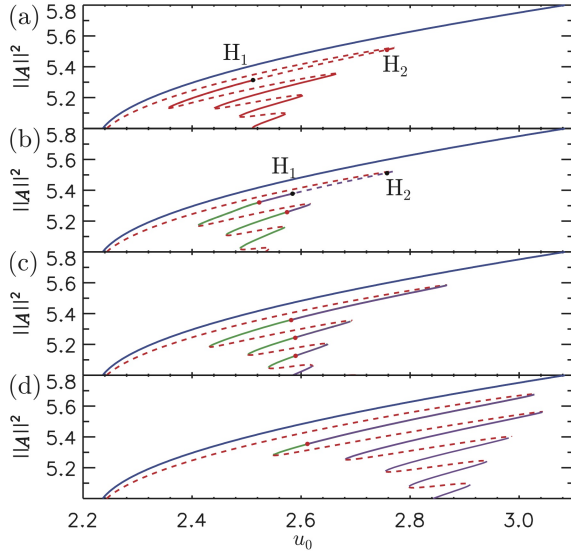


Fig. 5. Bifurcation diagrams for $\theta = 5$ at different values of $d_3 = 0$ (a), 0.2 (b), 0.3 (c), 0.7 (d). $H_{1,2}$ correspond to Hopf bifurcations (black dots). Solid (dashed) lines stand for stable (unstable) states. In solid purple (green) lines we refer to states with positive (negative) velocity. Solid red lines (for $d_3 = 0$) and red dots indicate zero velocity.

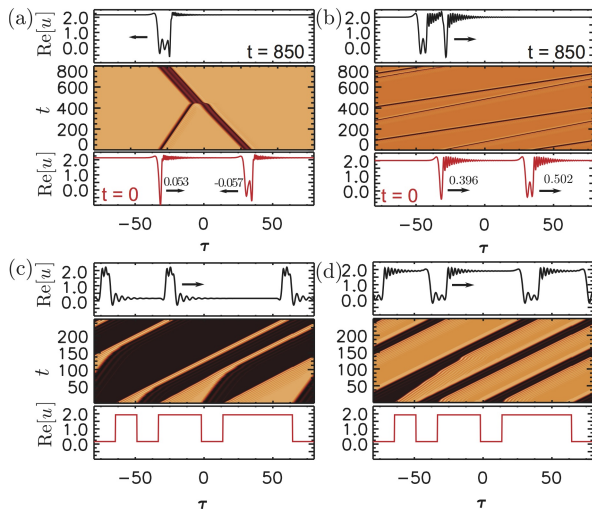


Fig. 6. Time evolution in the LLE (1) of an initial condition (in red) corresponding to: (a)-(b) two dark solitons traveling at different speeds; and (c)-(d) a distribution of three SW_u and SW_d such that the system is in the top and bottom HSS in 50% of the domain. The profile of the final stable, traveling structure is shown in black. Parameter sets: (a) $(\theta, u_0, d_3) = (5, 2.55, 0.2)$, (b) $(\theta, u_0, d_3) = (5, 2.8, 0.4)$, (c) $(\theta, u_0, d_3) = (4, 2.26, 0.7)$, (d) $(\theta, u_0, d_3) = (4, 2.36, 0.7)$.

23. P. Parra-Rivas, D. Gomila, F. Leo, S. Coen, L. Gelens, *Optics Letters* **39**, 2971–2974 (2014).
24. A. Mussot, E. Louvergneaux, N. Akhmediev, F. Reynaud, L. Delage, and M. Taki, “Optical fiber systems are convectively unstable,” *Phys. Rev. Lett.* **101**, 113904 (2008).
25. F. Leo, A. Mussot, P. Kockaert, Ph. Emplit, M. Haelterman, and M. Taki, “Nonlinear symmetry breaking induced by third-order dispersion in optical fiber cavities,” *Phys. Rev. Lett.* **110**, 104103 (2013).
26. J. K. Jang, S. G. Murdoch, S. Coen, and M. Erkintalo, *Observation of dispersive-wave emission by temporal cavity solitons* (CLEO/Europe, Munich, Germany, 2013), pp. PD–B.7.
27. S. Wang and X. Zeng, “Dispersive wave emission from dark solitons in microresonator-based Kerr frequency combs”, arXiv:1511.03023v1
28. F. Leo, S. Coen, P. Kockaert, S.-P. Gorza, Ph. Emplit, and M. Haelterman, *Nature Photon.* **4**, 471–476 (2010).
29. P. Colet, M. A. Matías, L. Gelens, and D. Gomila, *Phys. Rev. E* **89**, 012914 (2014).
30. L. Gelens, M. A. Matías, D. Gomila, T. Dorissen, and P. Colet, *Phys. Rev. E* **89**, 012915 (2014).

References

1. L. A. Lugiato and R. Lefever, “Spatial dissipative structures in passive optical systems,” *Phys. Rev. Lett.* **58**, 2209–2211 (1987).
2. P. Del’Haye, A. Schliesser, O. Arcizet, T. Wilken, R. Holzwarth, and T. J. Kippenberg, “Optical frequency comb generation from a monolithic microresonator,” *Nature* **450**, 1214–1217 (2007).
3. V. Brasch, M. Geiselmann, T. Herr, G. Lihachev, M. H. P. Pfeiffer, M. L. Gorodetsky, and T. J. Kippenberg, “Photonic chip-based optical frequency comb using soliton Cherenkov radiation,” *Science* **351**, 357 (2016).
4. T. J. Kippenberg, R. Holzwarth, and S. A. Diddams, “Microresonator-based optical frequency combs,” *Science* **332**, 555–559 (2011).
5. Y. Okawachi, K. Saha, J. S. Levy, Y. H. Wen, M. Lipson, and A. L. Gaeta, “Octave-spanning frequency comb generation in a silicon nitride chip,” *Opt. Lett.* **36**, 3398–3400 (2011).
6. S. B. Papp, K. Beha, P. Del’Haye, F. Quinlan, H. Lee, K. J. Vahala, and S. A. Diddams, “Microresonator frequency comb optical clock,” *Optica* **1**, 10–14 (2014).
7. F. Ferdous, H. Miao, D. E. Leaird, K. Srinivasan, J. Wang, L. Chen, L. T. Varghese, and A. M. Weiner, “Spectral line-by-line pulse shaping of on-chip microresonator frequency combs,” *Nature Photon.* **5**, 770–776 (2011).
8. T. Herr, K. Hartinger, J. Riemensberger, C. Y. Wang, E. Gavartin, R. Holzwarth, M. L. Gorodetsky, and T. J. Kippenberg, “Universal formation dynamics and noise of Kerr-frequency combs in microresonators,” *Nature Photon.* **6**, 480–487 (2012).
9. J. Pfeifle, V. Brasch, M. Lauer, Y. Yu, D. Wegner, T. Herr, K. Hartinger, P. Schindler, J. Li, D. Hillerkuss, R. Schmogrow, C. Weimann, R. Holzwarth, W. Freude, J. Leuthold, T. J. Kippenberg, and C. Koos, “Coherent terabit communications with microresonator Kerr frequency combs,” *Nature Photon.* **8**, 375–380 (2014).
10. S. Coen, H. G. Randle, T. Sylvestre, and M. Erkintalo, “Modeling of octave-spanning Kerr frequency combs using a generalized mean-field Lugiato-Lefever model,” *Opt. Lett.* **38**, 37–39 (2013).
11. Y. K. Chembo and C. R. Menyuk, “Spatiotemporal Lugiato-Lefever formalism for Kerr-comb generation in whispering-gallery-mode resonators,” *Phys. Rev. A* **87**, 053852 (2013).
12. F. Leo, L. Gelens, P. Emplit, M. Haelterman, and S. Coen, “Dynamics of one-dimensional Kerr cavity solitons,” *Opt. Expr.* **21**, 9180 (2013).
13. P. Parra-Rivas, D. Gomila, M. A. Matías, S. Coen, and L. Gelens, “Dynamics of localized and patterned structures in the Lugiato-Lefever equation determine the stability and shape of optical frequency combs,” *Phys. Rev. A* **89**, 043813 (2014).
14. C. Godey, I. V. Balakireva, A. Coillet, and Y. K. Chembo, “Stability analysis of the spatiotemporal Lugiato-Lefever model for Kerr optical frequency combs in the anomalous and normal dispersion regimes,” *Phys. Rev. A* **89**, 063814 (2014).
15. V.E. Lobanov, G. Lihachev, T. J. Kippenberg, and M.L. Gorodetsky, “Frequency combs and platicons in optical microresonators with normal GVD,” *Opt. Expr.* **23**, 7713–7721 (2015).
16. P. Parra-Rivas, D. Gomila, E. Knobloch, S. Coen and L. Gelens, “Origin and stability of dark pulse Kerr combs in normal dispersion resonators,” *Opt. Lett.* **41**, 2402–2405 (2016).
17. P. Parra-Rivas, E. Knobloch, D. Gomila, L. Gelens, “Dark solitons in the Lugiato-Lefever equation with normal dispersion,” *Phys. Rev. A* **93**, 063839 (2016).
18. W. Liang, A. A. Savchenkov, V. S. Ilchenko, D. Eliyahu, D. Seidel, A. B. Matsko, and L. Maleki, “Generation of a coherent near-infrared Kerr frequency comb in a monolithic microresonator with normal GVD,” *Opt. Lett.* **39**, 2920–2923 (2014).
19. S.-W. Huang, H. Zhou, J. Yang, J. F. McMillan, A. Matsko, M. Yu, D.-L. Kwong, L. Maleki, and C. W. Wong, “Mode-locked ultrashort pulse generation from on-chip normal dispersion microresonators,” *Phys. Rev. Lett.* **114**, 053901 (2015).
20. X. Xue, Y. Xuan, Y. Liu, P.-H. Wang, S. Chen, J. Wang, D. E. Leaird, M. Qi, and A. M. Weiner, “Mode-locked dark pulse Kerr combs in normal-dispersion microresonators,” *Nature Photon.* **9**, 594–600 (2015).
21. M. Tlidi and L. Gelens, “High-order dispersion stabilizes dark dissipative solitons in all-fiber cavities,” *Opt. Lett.* **35**, 306 (2010).
22. C. Milián and D. Skryabin, “Soliton families and resonant radiation in a micro-ring resonator near zero group-velocity dispersion,” *Opt. Expr.* **22**, 3732–3739 (2014).
23. P. Parra-Rivas, D. Gomila, F. Leo, S. Coen, L. Gelens, “Third-order chromatic dispersion stabilizes Kerr frequency combs,” *Optics Letters* **39**, 2971–2974 (2014).
24. A. Mussot, E. Louvergneaux, N. Akhmediev, F. Reynaud, L. Delage, and M. Taki, “Optical fiber systems are convectively unstable,” *Phys. Rev. Lett.* **101**, 113904 (2008).
25. F. Leo, A. Mussot, P. Kockaert, Ph. Emplit, M. Haelterman, and M. Taki, “Nonlinear symmetry breaking induced by third-order dispersion in optical fiber cavities,” *Phys. Rev. Lett.* **110**, 104103 (2013).
26. J. K. Jang, S. G. Murdoch, S. Coen, and M. Erkintalo, *Observation of dispersive-wave emission by temporal cavity solitons* (CLEO/Europe, Munich, Germany, 2013), pp. PD–B.7.
27. S. Wang and X. Zeng, “Dispersive wave emission from dark solitons in microresonator-based Kerr frequency combs”, arXiv:1511.03023v1
28. F. Leo, S. Coen, P. Kockaert, S.-P. Gorza, Ph. Emplit, and

- M. Haelterman, "Temporal cavity solitons in one-dimensional Kerr media as bits in an all-optical buffer," *Nature Photon.* **4**, 471–476 (2010).
29. P. Colet, M. A. Matías, L. Gelens, and D. Gomila, "Formation of localized structures in bistable systems through nonlocal spatial coupling. I. general framework," *Phys. Rev. E* **89**, 012914 (2014).
 30. L. Gelens, M. A. Matías, D. Gomila, T. Dorissen, and P. Colet, "Formation of localized structures in bistable systems through nonlocal spatial coupling. II. the nonlocal ginzburg-landau equation," *Phys. Rev. E* **89**, 012915 (2014).